Adsorption and diffusion of Au, Pt, and Co adatoms on $SrTiO_3$(001) surfaces: A density functional theory study

J. Buchwald[a,b,*], M. Hennes[c,1]

[a]*Institute for Materials Science and Max Bergmann Center of Biomaterials, TU Dresden, 01069, Dresden, Germany*
[b]*Helmholtz Centre for Environmental Research UFZ, Permoserstraße 15, 04318 Leipzig, Germany*
[c]*Sorbonne Université, CNRS, Institut des NanoSciences de Paris, INSP, 4 place Jussieu, 75005 Paris, France*

Abstract

We use Density Functional Theory (DFT) and Hubbard-model-based DFT+U calculations to determine preferential adsorption sites and energies of single, isolated Au, Pt, and Co atoms on planar $SrTiO_3$(001) surfaces. Based on these results, we employ a nudged elastic band (NEB) approach to calculate relevant diffusion energy barriers for the three transition metal species on SrO and TiO_2 terminated surfaces. This provides valuable quantitative input for future experimental and simulation studies and a sound basis to guide research aiming at controlling the microstructure of transition-metal-doped $SrTiO_3$ thin films.

Keywords: $SrTiO_3$, Surface diffusion, DFT

1. Introduction

Transition metal atom doping is a versatile approach that can be used to tailor the optical, catalytic, magnetic, and electrical transport properties of $SrTiO_3$. While stoichiometric $SrTiO_3$ crystallizes in a cubic perovskite structure, which, at room temperature, behaves as a diamagnetic, paraelectric insulator with a large band gap, addition of small amounts of impurity atoms can have a dramatic impact on the physical and chemical properties of this functional oxide. Prominent and technologically relevant examples are the creation of n-type conductivity *via* introduction of Nb [1, 2], formation of ferromagnetic thin films by addition of Co [3, 4, 5], Ni [6] or Mn [7], doping for memresistive applications [8, 9] or the use of small amounts of Cr [10, 11], Rh and Ir [12, 13, 14] for photoelectrochemical water splitting in the visible spectrum.

Molecular beam epitaxy (MBE) and pulsed laser deposition (PLD) based approaches have been routinely employed to obtain doped $SrTiO_3$ thin films with tunable composition and good structural quality. In contrast to ion bombardment, adding the dopant species during growth does not damage the thin films nor require subsequent annealing steps [15, 16]. However, the introduction of metal atoms during synthesis raises questions about their spatial distribution in the surrounding oxide. Depending on the growth conditions, the system might exhibit phase separation tendencies, and the added transition metals can form metallic precipitates, which will impact the final functionality of the thin film. For some applications, this clustering of metal atoms might be seen as a detrimental side effect, that needs to be avoided. However, it can also be sought after, when one is interested in the synthesis of $SrTiO_3$ thin films with nanocomposite structure [6, 17, 18, 19, 20].

In order to guide experimental research and obtain thin films with the desired microstructure, knowledge of the diffusion properties of dopant adatoms on $SrTiO_3$ surfaces is required. If the in-plane mobility during synthesis is low and the thin film growth velocity is high enough, the system will very likely incorporate the dopants as isolated atoms. On the contrary, fast diffusion will increase the propensity for phase separation to occur. To address this problem quantitatively, one requires information about the adsorption sites and diffusion pathways of metal atoms on $SrTiO_3$ surfaces. Surprisingly, this has not been studied in detail yet. While computational data are available describing the adsorption and diffusion of a variety of elements on other prototypical oxides, like MgO for example [21, 22, 23], only few studies on $SrTiO_3$ have been performed yet. Adsorption energies were calculated for Pt and Au on $SrTiO_3$, but the problem has not been addressed for Co adatoms [24, 25]. With regard to diffusion, the emphasis was predominantly put on pure $SrTiO_3$ growth [26, 27]. Recently, an attempt has been made to perform calculations for a Ni atom on $SrTiO_3$ [18].

To fill this gap, we scrutinize Co, Pt and Au adatom diffusion on planar strontium titanate (STO) (001) surfaces using a computational approach based on density functional theory (DFT), with particular emphasis on the

*Corresponding author
Email addresses: joerg.buchwald@ufz.de (J. Buchwald), marcel.hennes@sorbonne-universite.fr (M. Hennes)
[1]Currently at: Sorbonne Université, CNRS, Laboratoire de Chimie Physique - Matière et Rayonnement (LCPMR), 4 place Jussieu, 75005 Paris, France

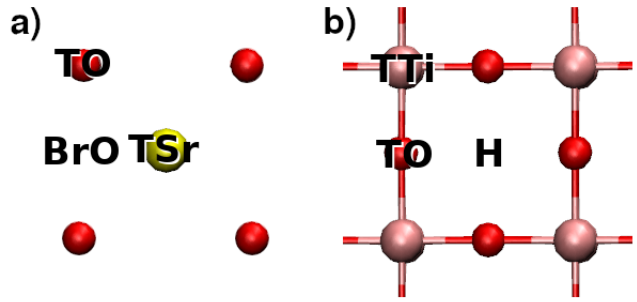

Figure 1: Binding sites on a (a) SrO- and (b) TiO_2- terminated STO surface: Sr atoms are shown in yellow (top-Sr sites labeled TSr), O atoms in red with top-oxygen sites (labeled TO), Ti atoms are shown in pink (top-Ti positions labeled TTi). Bridge oxygen positions (BrO) on the SrO termination and fourfold hollow sites (H) on the TiO_2 surface are shown as well (color online).

relevance of the (DFT+U) formalism. We will start the following sections by giving an overview of our computational methods and then proceed with a description of our results. These will consist of a detailed presentation of adsorption sites and energy barriers for both terminations. We will then close this work with a brief discussion of the results before turning to the summary and conclusion.

2. Computational details

All DFT calculations were carried out using the Quantum Espresso software package [28] with ultrasoft pseudopotentials and PBE-GGA exchange correlation [29, 30]. The kinetic energy cutoff was set to 35 Ry, while the charge density cutoff was chosen to be 500 Ry. The integration over the Brillouin zone was performed with a $3\times3\times1$ Monkhorst-Pack mesh [31]. By optimizing the unit cell and atom positions, we computed a value of $a_0^{\mathrm{STO}} = 3.923\,\text{Å}$ as bulk lattice constant which is in good agreement with earlier reported experimental and computed values for the PBE functional [32]. The simulation cell employed in our study consisted of a single STO-cube with volume $3a_0^{\mathrm{STO}}\times3a_0^{\mathrm{STO}}\times3a_0^{\mathrm{STO}}$ and periodic boundary conditions in-plane, combined with 3 a_0^{STO} vacuum inserted in z direction to create a (001) surface. The $SrTiO_3$ surface was structurally relaxed using the BFGS algorithm [33, 34, 35, 36] until the force components on every atom were less than $10^{-3}\mathrm{Ry/a_0}^2$, and changes in the total energy were found smaller than 10^{-4}Ry. Single Au, Co, and Pt atoms were placed at various canonical positions (*e.g.*, on top of oxygen atoms or at bridge positions between two oxygen atoms, as shown in Fig. 1) corresponding to a surface coverage $\theta = 1/9$. Keeping the lower atom layer fixed, we performed further geometry optimization on the system. For all cells containing magnetic Co atoms, we used a spin-polarized calculation scheme. Adsorption energies were calculated using

$$E_a = E_{\mathrm{total}} - E_{\mathrm{STO}} - E_{\mathrm{m}} \quad (1)$$

where E_{total} is the energy of the adsorbed system, E_{STO}, the energy of the clean STO surface and E_{m} the energy of a single metal atom (*i.e.*, Au, Pt, Co). To compute the height of the energy barriers, we employed the nudged elastic band (NEB) method with a Climbing Image (CI) scheme as implemented in Quantum Espresso to assess the height of the energy barrier. For the open-shell 3d and 5d metals Co and Pt, the results were additionally computed by means of DFT+U calculations using a Hubbard U correction from linear response [37] to overcome the problem of over-delocalization in these systems. Due to different system configurations of the adatom sites, different values of U were obtained. For Co, we found U to be within 4.6-4.9 eV and for Pt between 2.8 eV and 3.3 eV. In this paper, we present the energies referring to maximum values of U only, as all energy differences were found to be less than 0.05 eV.

3. Results and Discussion

For both common surface terminations, we explored typical binding sites for Au, Pt, and Co atoms in order to get appropriate minimal energy configurations as starting points for the NEB calculations (Fig. 1). In Tables 1-3 we list the computed adsorption energies as well as the corresponding next neighbor distances. A detailed description of these results and comparison with literature data will be provided in the remainder of this section.

Table 1: Adsorption energies and next-neighbor distances computed for different Au adatom arrangements on SrO- and TiO_2-terminated surfaces.

SrO termination

site	E_{a}(eV)	$d_{\mathrm{Au-O}}$ (Å)	$d_{\mathrm{Au-Sr}}$ (Å)	$d_{\mathrm{Au-Ti}}$ (Å)
TO	1.37	2.19	3.32	–
BrO	1.41	3.4	3.2	–

TiO_2 termination

site	E_{a}(eV)	$d_{\mathrm{Au-O}}$ (Å)	$d_{\mathrm{Au-Sr}}$ (Å)	$d_{\mathrm{Au-Ti}}$ (Å)
H	0.6	2.21	3.49	3.27

3.1. SrO-terminated surface

For the SrO-terminated surface, we identified the top oxygen positions (TO) as local minimal energy points for all three transition metal species. For Au, the direct TO position is nearly equally favorable to a distorted TO position, forming an O-O-Au angle of 66.4 degrees, a configuration which has not been reported so far [38]. The Pt

[2] Here, $\mathrm{a_0}$ denotes the bohr radius.

position appears also slightly distorted in the TiO plane, forming an O-O-Pt angle of 61 degrees with the nearby oxygen, which also contrasts with earlier results [39], where no such distortion was reported. This might be related to the symmetric monolayer arrangements used in [39] and the tiny activation barrier we found, between the minimal position and the high symmetry TO configuration, mainly when no +U correction is applied. In contrast, we find that the Co adatom sits directly on top of the oxygen atom.
From a quantitative perspective, our results are in reasonable agreement with available literature data. In the TO position, the adhesion energy of Au and the Au-O bond length (Table 1) are close to the results given by Wei *et al.*: $E_{\mathrm{ads}} = 1.26\,\mathrm{eV}$ and $d_{\mathrm{Au-O}} = 2.17\,\text{Å}$ [24]. Note that the difference in bond length is around 1%, while the binding energies differ by more than 8%. The discrepancy is more pronounced for Pt (Table 2), where Asthagiri and Sholl report $E_{\mathrm{ads}} = 2.77$ eV and $d_{\mathrm{Pt-O}} = 1.97$ Å for a TO site position in their GGA calculations [25]. This corresponds to a difference of roughly 2% in bond length and up to 30% difference in the binding energies. We emphasize, however, that those earlier calculations were performed for significantly larger surface coverage of the Pt atoms ($\theta = 0.25$). In fact, for Au as well as for Pt on $SrTiO_3$, it has been shown that a decrease of θ correlates with higher adsorption energy [24, 25]. In addition to the TO positions, we identified BrO sites for the Au and Pt adatoms as minimum energy positions (Table 1-2). Surprisingly, for Au, the energy of this bridge site is slightly lower than the TO position. This clearly challenges earlier findings, where the TO placement of the Au adatom was identified as the global minimum of the system [24]. It is interesting to notice that in the same study, the authors analyzed a similar adsorption configuration, substituting a single subsurface Ti atom by Nb. This gave rise to BrO minimum energy configurations, identical to the one observed in the present case. Considering that both configurations are very close in energy ($\Delta E = 40$ meV), we might attribute the observed discrepancy to a different relaxation of the surface. This, again, might be traced back to the amount of Au surface coverage. For the Pt atom, we also identified BrO sites as local minima. However, in contrast to Au, their energy is larger by approximately 0.9 eV. Thus, as already described in earlier studies, we conclude that the TO position represents the preferential binding site [39]. Finally, we find a qualitatively different behavior for the Co-adatom, which tends to bind to both near-by oxygen atoms. This gives rise to an additional minimum located between the TO and the BrO positions, which is very similar to what has been observed for Ni adsorption on SrO terminated $SrTiO_3$ surface [18].

Having identified preferential adsorption sites, we now turn to the description of diffusion barriers on SrO - terminated surfaces. These were computed using NEB-CI calculations with one to five intermediate images. For paths containing more than two relevant minimal points, the path was split into segments and reassembled afterwards. The resulting lowest energy paths are given in Fig. 2 - 4. For the Au adatom, the minimum energy diffusion path connects two BrO positions via a TO site. The activation barrier between the BrO and the TO position is found to be small $E_{\mathrm{act}} = 0.1$ eV and lies on the same energy level as the distorted 'TO' positions (I1) (Fig. 2). While these were also found to be minimal positions, they are not identified as such in the NEB diagram. We thus conclude that the activation barrier I1→BrO is negligible compared to the global barrier of BrO→TO.
For Pt, as already emphasized, the minimal state consists in a slightly shifted TO position (Fig. 3). A change of orientation with respect to the oxygen atom is related to the crossing of a small barrier of 0.03 eV (GGA+U: 0.13 eV) from TO1 to TO2. To jump from one oxygen atom to another, a barrier of 1.0 eV (GGA+U: 1.04 eV) has to be overcome. The BrO position serves as an intermediate minimum. Similar to the case of Au diffusion, the Pt adatom can escape this minimum by crossing an energy barrier of 0.15 eV (GGA+U: 0.05 eV). Finally, the behavior of the Co atom is qualitatively different. While the diffusion path connects two TO positions, intermediate steps involve twofold coordinated sites. The reaction barrier height equals $E_{\mathrm{act}} = 0.75$ eV (GGA+U: 1.24 eV) from the one-oxygen coordinated TO to the two oxygen coordinated I2 minimum position (Fig. 4). The transition between the two equivalent two-coordinated states I2 and

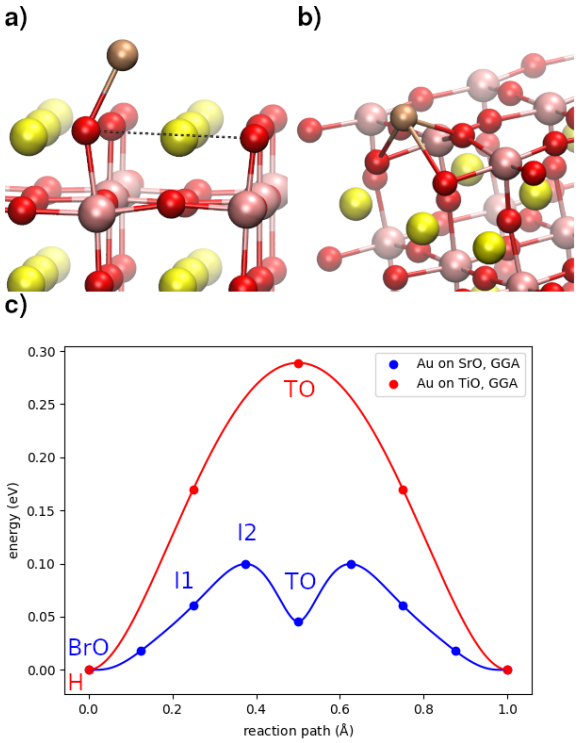

Figure 2: a) TO minimal configuration of an Au adatom on SrO-terminated STO. b) H minimal configuration of Au on TiO_2-terminated STO. c) Lowest energy paths of Au adatoms on a SrO (blue) and a TiO_2 (red) -terminated STO surface.

Table 2: Adsorption energies and next-neighbor distances computed for different Pt adatom arrangements on SrO- and TiO_2-terminated surfaces.

SrO termination

site	E_a(eV)	E_a^{+U}(eV)	d_{Pt-O} (Å)	d_{Pt-Sr} (Å)	d_{Pt-Ti} (Å)
TO	3.66	3.01	1.93	3.16	–
BrO	2.74	2.02	2.12	2.7	–

TiO_2 termination

site	E_a(eV)	E_a^{+U}(eV)	d_{Pt-O} (Å)	d_{Pt-Sr} (Å)	d_{Pt-Ti}
H	4.16	3.52	2.05	2.91	2.94
TO	2.87	2.14	1.97	–	2.84
O–PT–O	4.27	3.23	2.03	3.21	2.43

Table 3: Adsorption energies and next-neighbor distances computed for different Co adatom arrangements on SrO- and TiO_2-terminated surfaces.

SrO termination

site	E_a(eV)	E_a^{+U}(eV)	d_{Co-O} (Å)	d_{Co-Sr} (Å)	d_{Co-Ti} (Å)
TO	1.64	1.03	1.80	3.56	–
O–Co–O	1.93	0.65	1.73	3.19	3.53

TiO_2 termination

site	E_a(eV)	E_a^{+U}(eV)	d_{Co-O} (Å)	d_{Co-Sr} (Å)	d_{Co-Ti} (Å)
H	3.81	3.03	1.97	3.03	3.04

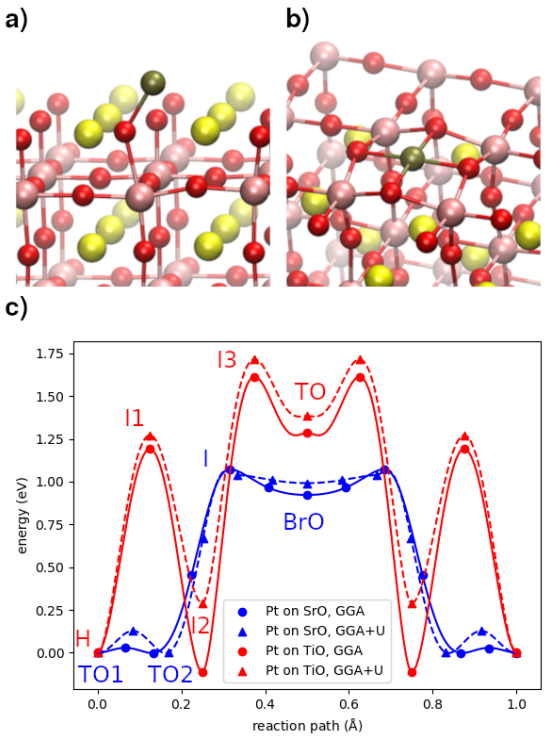

Figure 3: a) TO minimal configuration of Pt adatom on SrO terminated STO. b) H minimal configuration of Pt on TiO_2 termnated STO. c) Lowest energy paths of Pt adatoms on a SrO (blue) and TiO_2 (red) -terminated STO surface.

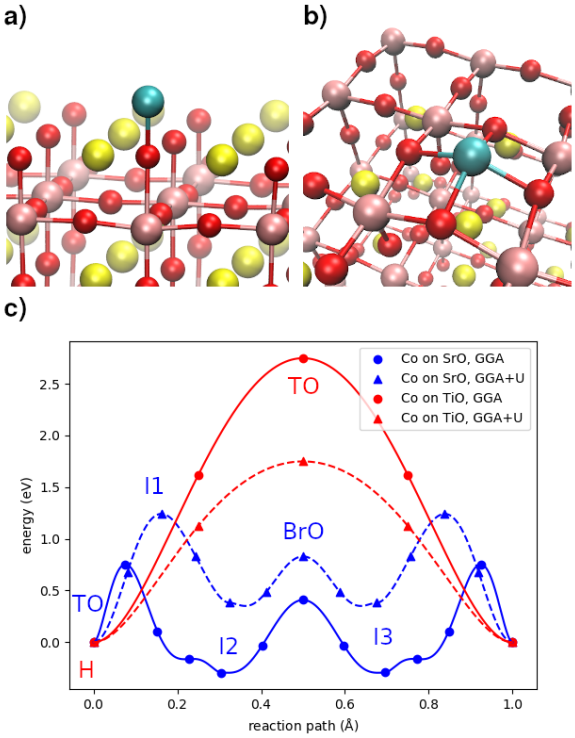

Figure 4: a) TO minimal configuration of Co adatom on SrO terminated STO. b) H minimal configuration of Co on TiO terminated STO. c) Lowest energy paths of Co adatoms on a SrO (blue) and TiO_2 (red) -terminated STO surface.

I3 is reached by crossing a barrier of $E = 0.7$ eV (GGA+U: 0.4 eV), passing over the BrO position, which, unlike for Au and Pt does not represent a local minimum. To eventually return to the original minimum state, *i.e.*, dissolving from one oxygen atom, a barrier of $E_{\text{act}} = 1.05$ eV (GGA+U: 0.76 eV) has to be overcome.

3.2. TiO_2-terminated surface

The adsorption behavior of Au, Pt, and Co on TiO_2 differs markedly from what we found on the SrO surface. In all three cases, a steep energy minimum was observed at the fourfold hollow site H. Note that such a fourfold coordinated minimum has also been reported for Ag and Ni adsorption on $SrTiO_3$ [18, 38]. With respect to the TO position that acts as a transition point between cells we find an energy difference of 0.29 eV for Au, 1.28 eV (GGA+U: 1.38 eV) for Pt and 2.75 eV (GGA+U: 1.75 eV) for Co between both states. For Au and Co, this position indeed corresponds to a global minimum (Table 1-3). In contrast for Pt, our GGA calculations suggest another, even lower-lying site. Pt atoms coordinated to two O-atoms yield an overall energy lower by 90 meV (Table 2). As will be shown later, this picture changes when using the more advanced DFT+U formalism. It is noteworthy that our results conflict with those presented in [25], where the TO site is claimed to be energetically preferred with an adsorption energy of 3.47 eV, while our calculations indicate $E_a = 2.87$ eV for the same site using the GGA approach.

As shown in Fig. 2 and Fig. 4, the diffusion paths of Au and Co adatoms exhibit a simple structure and are characterized by a single saddle point. The hopping from one STO unit cell to the adjacent one happens via the TO position for Au and Co (Fig. 2 and 4), a transition that is reminiscent of the diffusion path of Ni on TiO_2-terminated STO [18]. For Au, the barrier height is small and amounts to 0.29 eV while we obtain a substantial barrier of 2.75 eV (GGA+U: 1.75 eV) for Co. A similarly high value was observed in the case of Ni diffusion on the same planar surface [18]. Qualitative differences in the energy landscape were found for Pt, where the diffusion path appears to be significantly more complex. In addition to the hollow site H, another minimum is observed at an intermediate state I2 in which Pt is linearly coordinated to two oxygen atoms, pulling one of them out of the surface. The jump between these two states requires to overcome a barrier of 1.19 eV (1.27 eV). Once trapped in the twofold coordinated state, the Pt atom can climb into a TO position by overcoming a barrier of 1.72 eV (GGA+U: 1.42 eV). In contrast to Au and Co, this configuration represents a local minimum with short dwell time, being separated from the adjacent minimum by a small barrier of 0.32 eV (0.33 eV). Unfortunately, data on the diffusion of Pt on $SrTiO_3$ is scarce. In references [40] and [41], a detailed study of

Pt_n cluster diffusion on anatase (101) TiO_2 is presented. For the case of $n = 1$, the authors identified minimal energy configurations corresponding to equally stable O-O bridge and O-Ti-O sites [41]. Diffusion barrier heights reported in this study ranged from 0.86 eV to 1.41 eV, which is surprisingly close to our findings despite the difference in the surface structure of the two systems.

3.3. DFT calculations vs. DFT+U

While DFT+U results have been given alongside DFT calculations throughout this paper, we close this section by providing additional remarks concerning the two approaches.

The use of the DFT+U approach appears relevant to us in the present context, as it efficiently compensates the effect of over-delocalization. A stronger impact is thus to be expected for highly localized 3d- when compared to 5d-metals, due to their more extended radial wave functions [42]. This is fully compatible with our simulation results. Indeed, adsorption energy diffusion calculations for Co and Pt reveal that the Hubbard U correction amounts to 20 percent in the adsorption energies of Pt while it can become as high as 40 percent in the case of Co. A clear impact on the height of the diffusion barriers is also evidenced. In the case of Pt, the correction is marginal but suggests that the H site is indeed the global minimum of the system. The DFT+U approach seems to have a substantial effect on the adsorption energies of Pt amounting to a difference of half an electronvolt and to the energy of the two-coordinated intermediate state while the structure stays nearly the same (GGA: $d(O_1Pt) = 2.05$ Å, $d(O_2Pt) = 2.0$ Å, $\angle O_1PtO_2 = 174.45°$, GGA+U: $d(O_1Pt) = 2.06$ Å, $d(O_2Pt) = 2.0$ Å, $\angle O_1PtO_2 = 174.48°$). In contrast, for Co adatom diffusion, we find pronounced differences between both approaches: While the DFT+U-calculations reveal only a small effect on the barrier heights of paramagnetic Pt, a significant impact on the diffusion energies of the magnetic Co adatom is unraveled, leading to a shift of global minimum positions on the SrO surface as well as a reduction of about 1 eV in the activation energy on the TiO_2 terminated surface (Fig. 4).

4. Summary and conclusion

The diffusion behavior of different transition metals (Au, Pt, Co) on STO(001) was investigated by means of first principle DFT calculations. Minimal positions for the adatoms were determined on both possible planar surface terminations, and representative diffusion paths were found using the NEB-CI method. We observe that (a) the choice of the $SrTiO_3$-termination has a large impact on the diffusion behavior of the adatoms, with enhanced mobility observed on the SrO surface, (b) Au diffuses much faster on $SrTiO_3$, than Co and Pt. With an activation barrier smaller than 0.3 eV, it can be surmised that Au atoms will more likely aggregate into clusters at the surface of the perovskite, even when deposited at moderate temperatures. And finally, (c) our study unravels the need to compensate over-delocalization effects to obtain a more reliable description of the diffusion properties of 3d metals such as Co.

Although doping of $SrTiO_3$ has evolved into a mature research field, computational approaches that are able to grasp the initial stages of thin film growth remain scarce. Coarse-grained kinetic Monte Carlo (KMC) computation schemes can serve as a viable tool to gain a better understanding of growth phenomena at oxide surfaces and unravel whether or not, aggregation of dopant atoms will take place. However, such studies require detailed information on the hopping probabilities of the surface atoms, which is difficult to assess experimentally. The data presented herein can thus provide a solid starting point for further computational investigations, ultimately aiming at obtaining a better understanding of processing parameters relevant to $SrTiO_3$ thin film doping.

5. Acknowledgements

Computing time provided by the Center for Information Services and High Performance Computing (ZIH), TU Dresden is gratefully acknowledged. M. H. acknowledges financial support from the French Embassy in Berlin (Service pour la Science et la Technologie) and Campus France.

[1] T. Tomio, H. Miki, H. Tabata, T. Kawai, S. Kawai, Control of electrical conductivity in laser deposited $SrTiO_3$ thin films with Nb doping, Journal of Applied Physics 76 (10) (1994) 5886–5890, doi:\bibinfo{doi}{10.1063/1.358404}.

[2] T. Zhao, H. Lu, F. Chen, S. Dai, G. Yang, Z. Chen, Highly conductive Nb doped $SrTiO_3$ epitaxial thin films grown by laser molecular beam epitaxy, Journal of Crystal Growth 212 (3) (2000) 451 – 455, doi:\bibinfo{doi}{https://doi.org/10.1016/S0022-0248(00)00307-9}.

[3] J. Lee, Z. Khim, Y. Park, D. Norton, N. Theodoropoulou, A. Hebard, J. Budai, L. Boatner, S. Pearton, R. Wilson, Magnetic properties of Co- and Mn-implanted $BaTiO_3$, $SrTiO_3$ and $KTaO_3$, Solid-State Electronics 47 (12) (2003) 2225 – 2230, doi:\bibinfo{doi}{https://doi.org/10.1016/S0038-1101(03)00202-8}.

[4] T. Fix, M. Liberati, H. Aubriet, S.-L. Sahonta, R. Bali, C. Becker, D. Ruch, J. L. MacManus-Driscoll, E. Arenholz, M. G. Blamire, Ferromagnetism in Co-doped (La,Sr)TiO_3, New Journal of Physics 11 (7) (2009) 073042, doi:\bibinfo{doi}{10.1088/1367-2630/11/7/073042}.

[5] D. H. Kim, L. Bi, P. Jiang, G. F. Dionne, C. A. Ross, Magnetoelastic effects in $SrTi_{1-x}M_xO_3$ (M = Fe, Co, or Cr) epitaxial thin films, Phys. Rev. B 84 (2011) 014416, doi:\bibinfo{doi}{10.1103/PhysRevB.84.014416}.

[6] V. Schuler, F. J. Bonilla, D. Demaille, A. Coati, A. Vlad, Y. Garreau, M. Sauvage-Simkin, A. Novikova, E. Fonda, S. Hidki, V. Etgens, F. Vidal, Y. Zheng, Huge metastable axial strain in ultrathin heteroepitaxial vertically aligned nanowires, Nano Research 8 (6) (2015) 1964–1974, doi:\bibinfo{doi}{10.1007/s12274-014-0706-1}.

[7] S. Middey, C. Meneghini, S. Ray, Evidence of oxygen-vacancy-induced ferromagnetic order in single crystal Mn-doped $SrTiO_3$, Applied Physics Letters 101 (4) (2012) 042406.

[8] M. Janousch, G. Meijer, U. Staub, B. Delley, S. Karg, B. Andreasson, Role of Oxygen Vacancies in Cr-Doped $SrTiO_3$ for Resistance-Change Memory, Advanced Materials 19 (17) (2007) 2232–2235, doi:\bibinfo{doi}{10.1002/adma.200602915}.

[9] R. Muenstermann, T. Menke, R. Dittmann, R. Waser, Coexistence of Filamentary and Homogeneous Resistive Switching in Fe-Doped $SrTiO_3$ Thin-Film Memristive Devices, Advanced Materials 22 (43) (2010) 4819–4822.

[10] H. Maruska, A. K. Ghosh, Transition-metal dopants for extending the response of titanate photoelectrolysis anodes, Solar Energy Materials 1 (3) (1979) 237 – 247, doi:\bibinfo{doi}{https://doi.org/10.1016/0165-1633(79)90042-X}.

[11] D. Wang, J. Ye, T. Kako, T. Kimura, Photophysical and Photocatalytic Properties of $SrTiO_3$ Doped with Cr Cations on Different Sites, The Journal of Physical Chemistry B 110 (32) (2006) 15824–15830.

[12] R. Konta, T. Ishii, H. Kato, A. Kudo, Photocatalytic activities of noble metal ion doped $SrTiO_3$ under visible light irradiation, The Journal of Physical Chemistry B 108 (26) (2004) 8992–8995.

[13] S. Kawasaki, K. Akagi, K. Nakatsuji, S. Yamamoto, I. Matsuda, Y. Harada, J. Yoshinobu, F. Komori, R. Takahashi, M. Lippmaa, C. Sakai, H. Niwa, M. Oshima, K. Iwashina, A. Kudo, Elucidation of Rh-Induced In-Gap States of Rh:$SrTiO_3$ Visible-Light-Driven Photocatalyst by Soft X-ray Spectroscopy and First-Principles Calculations, The Journal of Physical Chemistry C 116 (46) (2012) 24445–24448, doi:\bibinfo{doi}{10.1021/jp3082529}.

[14] S. Kawasaki, R. Takahashi, K. Akagi, J. Yoshinobu, F. Komori, K. Horiba, H. Kumigashira, K. Iwashina, A. Kudo, M. Lippmaa, Electronic structure and photoelectrochemical properties of an Ir-doped SrTiO3 photocatalyst, The Journal of Physical Chemistry C 118 (35) (2014) 20222–20228.

[15] P. Moretti, B. Canut, S. Ramos, P. Thevenard, G. Godefroy, Niobium implantation effects in $BaTiO_3$ and $SrTiO_3$, Nuclear Instruments and Methods in Physics Research Section B: Beam Interactions with Materials and Atoms 65 (1) (1992) 264 – 269, doi:\bibinfo{doi}{https://doi.org/10.1016/0168-583X(92)95046-T}.

[16] S. Thevuthasan, W. Jiang, V. Shutthanandan, W. Weber, Accumulation and thermal recovery of disorder in Au^{2+}-irradiated $SrTiO_3$, Journal of Nuclear Materials 289 (1) (2001) 204 – 209, doi:\bibinfo{doi}{https://doi.org/10.1016/S0022-3115(00)00699-1}.

[17] S. Kawasaki, R. Takahashi, T. Yamamoto, M. Kobayashi, H. Kumigashira, J. Yoshinobu, F. Komori, A. Kudo, M. Lippmaa, Photoelectrochemical water splitting enhanced by self-assembled metal nanopillars embedded in an oxide semiconductor photoelectrode, Nature Communications 7 (2016) 11818.

[18] M. Hennes, V. Schuler, X. Weng, J. Buchwald, D. Demaille, Y. Zheng, F. Vidal, Growth of vertically aligned nanowires in metaloxide nanocomposites: kinetic Monte-Carlo modeling versus experiments, Nanoscale 10 (2018) 7666–7675, doi:\bibinfo{doi}{10.1039/C7NR08974K}.

[19] X. Weng, M. Hennes, A. Coati, A. Vlad, Y. Garreau, M. Sauvage-Simkin, E. Fonda, G. Patriarche, D. Demaille, F. Vidal, Y. Zheng, Ultrathin Ni nanowires embedded in $SrTiO_3$: Vertical epitaxy, strain relaxation mechanisms, and solid-state amorphization, Phys. Rev. Materials 2 (2018) 106003, doi:\bibinfo{doi}{10.1103/PhysRevMaterials.2.106003}.

[20] M. Lippmaa, S. Kawasaki, R. Takahashi, T. Yamamoto, Noble metal clustering and nanopillar formation in an oxide matrix, Japanese Journal of Applied Physics 59 (1) (2019) 010501, doi:\bibinfo{doi}{10.7567/1347-4065/ab57e2}.

[21] I. Yudanov, G. Pacchioni, K. Neyman, N. Rösch, Systematic Density Functional Study of the Adsorption of Transition Metal Atoms on the MgO(001) Surface, The Journal of Physical Chemistry B 101 (15) (1997) 2786–2792, doi:\bibinfo{doi}{10.1021/jp962487x}.

[22] Y.-L. Hu, W.-B. Zhang, Y.-H. Deng, B.-Y. Tang, Initial stage of Ag deposition on regular MgO(001) surface: A DFT study, Computational Materials Science 42 (1) (2008) 43 – 49, doi:\bibinfo{doi}{https://doi.org/10.1016/j.commatsci.2007.06.006}.

[23] Y. Shim, J. G. Amar, Ab initio study of early stage Nb growth on MgO(001), Surface Science 645 (2016) 80 – 87, doi:\bibinfo{doi}{https://doi.org/10.1016/j.susc.2015.11.013}.

[24] W. Wei, Y. Dai, M. Guo, B. Huang, Au adsorption and Au-mediated charge transfer on the SrO-termination of SrTiO3 (001) surface, Applied Surface Science 257 (15) (2011) 6607 – 6611, doi:\bibinfo{doi}{https://doi.org/10.1016/j.apsusc.2011.02.086}.

[25] A. Asthagiri, D. S. Sholl, DFT study of Pt adsorption on low index $SrTiO_3$ surfaces: $SrTiO_3$(100), $SrTiO_3$(111) and $SrTiO_3$(110), Surface Science 581 (1) (2005) 66 – 87, doi:\bibinfo{doi}{https://doi.org/10.1016/j.susc.2005.02.033}.

[26] H. Guhl, W. Miller, K. Reuter, Oxygen adatoms at $SrTiO_3$(001): A density-functional theory study, Surface Science 604 (3-4) (2010) 372 – 376, doi:\bibinfo{doi}{https://doi.org/10.1016/j.susc.2009.11.033}.

[27] M. Hong, J. L. Wohlwend, R. K. Behera, S. R. Phillpot, S. B. Sinnott, B. P. Uberuaga, Surface diffusion on $SrTiO_3$ (100): A temperature accelerated dynamics and first principles study, Surface Science 617 (2013) 237 – 241, doi:\bibinfo{doi}{https://doi.org/10.1016/j.susc.2013.08.002}.

[28] P. Giannozzi, S. Baroni, N. Bonini, M. Calandra, R. Car, C. Cavazzoni, D. Ceresoli, G. L. Chiarotti, M. Cococcioni, I. Dabo, A. D. Corso, S. de Gironcoli, S. Fabris, G. Fratesi, R. Gebauer, U. Gerstmann, C. Gougoussis, A. Kokalj, M. Lazzeri, L. Martin-Samos, N. Marzari, F. Mauri, R. Mazzarello, S. Paolini, A. Pasquarello, L. Paulatto, C. Sbraccia, S. Scandolo, G. Sclauzero, A. P. Seitsonen, A. Smogunov, P. Umari, R. M. Wentzcovitch, QUANTUM ESPRESSO: a modular and open-source software project for quantum simulations of materials, Journal of Physics: Condensed Matter 21 (39) (2009) 395502.

[29] J. P. Perdew, K. Burke, M. Ernzerhof, Generalized Gradient Approximation Made Simple, Phys. Rev. Lett. 77 (1996) 3865–3868, doi:\bibinfo{doi}{10.1103/PhysRevLett.77.3865}.

[30] Y. Zhang, W. Yang, Comment on "Generalized Gradient Approximation Made Simple", Phys. Rev. Lett. 80 (1998) 890–890, doi:\bibinfo{doi}{10.1103/PhysRevLett.80.890}.

[31] H. J. Monkhorst, J. D. Pack, Special points for Brillouin-zone integrations, Physical Review B 13 (12) (1976) 5188.

[32] S. Piskunov, E. Heifets, R. Eglitis, G. Borstel, Bulk properties and electronic structure of SrTiO3, BaTiO3, PbTiO3 perovskites: an ab initio HF/DFT study, Computational Materials Science 29 (2) (2004) 165–178.

[33] C. G. Broyden, The Convergence of a Class of Double-rank Minimization Algorithms 1. General Considerations, IMA Journal of Applied Mathematics 6 (1) (1970) 76, doi:\bibinfo{doi}{10.1093/imamat/6.1.76}.

[34] R. Fletcher, A new approach to variable metric algorithms, The Computer Journal 13 (3) (1970) 317, doi:\bibinfo{doi}{10.1093/comjnl/13.3.317}.

[35] D. Goldfarb, A family of variable-metric methods derived by variational means, Mathematics of computation 24 (109) (1970) 23–26.

[36] D. F. Shanno, Conditioning of quasi-Newton methods for function minimization, Mathematics of computation 24 (111) (1970) 647–656.

[37] M. Cococcioni, S. de Gironcoli, Linear response approach to the calculation of the effective interaction parameters in the LDA + U method, Phys. Rev. B 71 (2005) 035105, doi:\bibinfo{doi}{10.1103/PhysRevB.71.035105}.

[38] W. Wei, Y. Dai, M. Guo, Y. Zhu, B. Huang, Density Functional Theory Study of Ag Adsorption on $SrTiO_3$ (001) Surface, The Journal of Physical Chemistry C 114 (24) (2010) 10917–10921, doi:\bibinfo{doi}{10.1021/jp102865r}.

[39] A. Asthagiri, D. S. Sholl, First principles study of Pt adhesion and growth on SrO- and TiO_2-terminated $SrTiO_3$(100), The Journal of Chemical Physics 116 (22) (2002) 9914–9925, doi:\bibinfo{doi}{10.1063/1.1476322}.

[40] C. Jin, Y. Dai, W. Wei, X. Ma, M. Li, B. Huang, Effects of single metal atom (Pt, Pd, Rh and Ru) adsorption on the pho-

tocatalytic properties of anatase TiO_2, Applied Surface Science 426 (2017) 639–646.

[41] Y. Zhou, C. L. Muhich, B. T. Neltner, A. W. Weimer, C. B. Musgrave, Growth of Pt particles on the anatase TiO_2 (101) surface, The Journal of Physical Chemistry C 116 (22) (2012) 12114–12123.

[42] G. Lan, J. Song, Z. Yang, A linear response approach to determine Hubbard U and its application to evaluate properties of $Y_2B_2O_7$, B = transition metals 3d, 4d and 5d, Journal of Alloys and Compounds 749 (2018) 909 – 925, doi:\bibinfo{doi}{https://doi.org/10.1016/j.jallcom.2018.03.336}.